SAND REPORT
SAND2003-4115
Unlimited Release
Printed November 2003

Arrayed Resonant Subwavelength Gratings LDRD 38618 Final Report

Shanalyn A. Kemme, David W. Peters, Joel R. Wendt, Tony R. Carter, Sally Samora, G. Ronald Hadley, Mial E. Warren, and Carter L. Grotbeck

Prepared by
Sandia National Laboratories
Albuquerque, New Mexico 87185 and Livermore, California 94550

Sandia is a multiprogram laboratory operated by Sandia Corporation,
a Lockheed Martin Company, for the United States Department of Energy's
National Nuclear Security Administration under Contract DE-AC04-94-AL85000.

Issued by Sandia National Laboratories, operated for the United States Department of Energy by Sandia Corporation.

Available to DOE and DOE contractors from
U.S. Department of Energy
Office of Scientific and Technical Information
P.O. Box 62
Oak Ridge, TN 37831

Telephone: (865)576-8401
Facsimile: (865)576-5728
E-Mail: reports@adonis.osti.gov
Online ordering: http://www.doe.gov/bridge

Available to the public from
U.S. Department of Commerce
National Technical Information Service
5285 Port Royal Rd
Springfield, VA 22161

Telephone: (800)553-6847
Facsimile: (703)605-6900
E-Mail: orders@ntis.fedworld.gov
Online order: http://www.ntis.gov/help/ordermethods.asp?loc=7-4-0#online

SAND 2003-4115
Unlimited Release
Printed November 2003

Arrayed Resonant Subwavelength Gratings
LDRD 38618 Final Report

Shanalyn A. Kemme, David W. Peters, Joel R. Wendt, Tony R. Carter, and Sally Samora
Photonic Microsystems Technologies Department

G. Ronald Hadley
R.F. Microsystems Technologies Department

Mial E. Warren
Microsystems Partnerships Department

Carter L. Grotbeck
Remote Sensing and Exploitation Department

Sandia National Laboratories
P.O. Box 5800 MS 0603
Albuquerque, NM 87185-0603

Abstract

This report describes a passive, optical component called resonant subwavelength gratings (RSGs), which can be employed as one element in an RSG array. An RSG functions as an extremely narrow wavelength and angular band reflector, or mode selector. Theoretical studies predict that the infinite, laterally-extended RSG can reflect 100% of the resonant light while transmitting the balance of the other wavelengths. Experimental realization of these remarkable predictions has been impacted primarily by fabrication challenges. Even so, we will present large area (1.0mm) RSG reflectivity as high as 100.2%, normalized to deposited gold.

Broad use of the RSG will only truly occur in an accessible micro-optical system. This program at Sandia is a normal incidence array configuration of RSGs where each array element resonates with a distinct wavelength to act as a dense array of wavelength- and mode-selective reflectors. Because of the array configuration, RSGs can be matched to an array of pixels, detectors, or chemical/biological cells for integrated optical sensing. Micro-optical system considerations impact the ideal, large area RSG performance by requiring finite extent devices and robust materials for the appropriate wavelength. Theoretical predictions and experimental measurements are presented that demonstrate the component response as a function of decreasing RSG aperture dimension and off-normal input angular incidence.

Acknowledgement

Sandia is a multiprogram laboratory operated by Sandia Corporation, a Lockheed Martin Company, for the United States Department of Energy's National Nuclear Security Administration under contract DE-AC04-94AL85000.

Table of Contents

Figures

1. Introduction

The described micro-optical system project employs an array of resonant subwavelength gratings (RSGs)[1-3], also known in the literature as guided mode resonance filters[4], corrugated dielectric waveguides[5], corrugated waveguides[6], and other variations. This optical component, shown in Figure 1, functions as an extremely narrow wavelength-, polarization, and angular-band reflector, or mode selector. Theoretical studies predict that the infinite, laterally extended component can reflect 100% of the resonant light while transmitting the balance of the other wavelengths. Experimental realization of these remarkable predictions has been impacted primarily by fabrication challenges. Broad use of this component will only truly occur in an accessible micro-optical system.

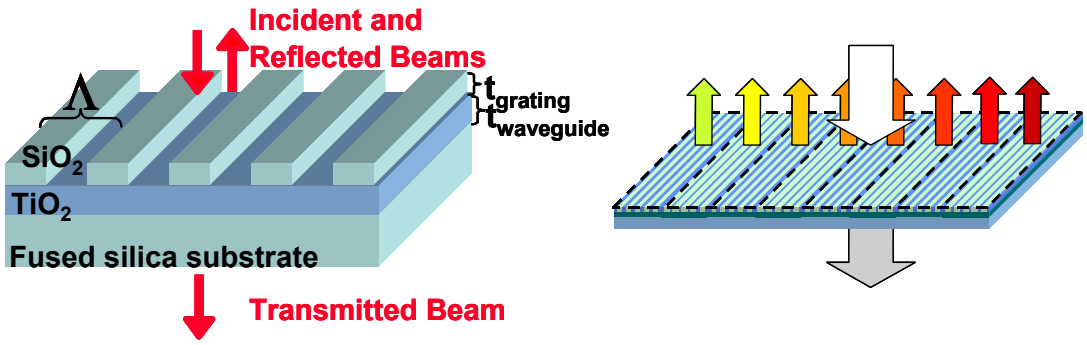

Figure 1 RSG single component and array-format schematic.

This program at Sandia is a normal incidence array configuration RSG where each array element resonates with a distinct wavelength to act as a dense array of wavelength-selective reflectors. Design goals are peak reflectance of unity, narrow spectral bandwidth, and low sideband reflectivity for use in an arrayed grating structure near the visible wavelength regime. The resulting design accomplishes these objectives over a broad range of 300nm by keeping all thicknesses and refractive indices constant and only lithographically varying the grating pitch from one RSG pixel to the next. The shift in resonant peak is linear with respect to grating pitch, as seen in Figure 2. At the center resonant wavelength of 850nm, the sidebands remain below 4.3%, allowing this RSG design to function well in an arrayed structure. The RSG simulation parameters are: $t_{grating}$ = 139nm, $t_{waveguide}$ = 185nm, n_{TiO2} = 2.15, n_{SiO2} = 1.45, Λ = 470nm[7].

Success of the RSG is highly dependent upon the quality of fabrication. Measured reflectivity of the RSG is potentially greater than that of a comparable linearly variable thin-film component. However, unlike thin films, the RSG filter parameters such as grating period may be abruptly altered in the lateral direction to realize a pixelated array of filters.

System and fabrication considerations for the RSG bound possible material and configuration choices. The device must work in the visible to near IR wavelength region, so that the substrate, waveguide, and grating must all be transparent in this wavelength regime. This precludes desirable high index contrast materials such as silicon or gallium arsenide based compounds.

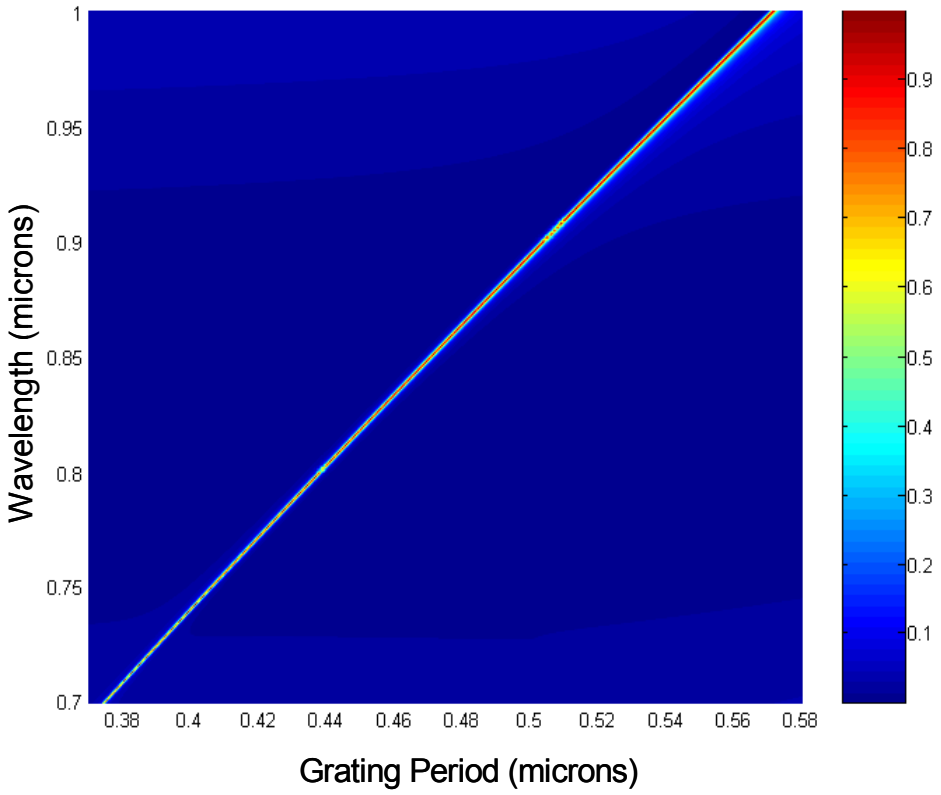

Figure 2 Linear RSG reflectivity response for a wavelength range of 0.7-1.0 μm as a function of grating period.

The working design utilizes a fused silica substrate, a TiO_2 waveguide, and a SiO_2 grating. The RSG will be in a linear array format, each pixel reflecting a different wavelength. Consequently, the RSG waveguide should only be thick enough to support one guided mode (within the spectral response of the array) or the array will reflect from multiple pixels when illuminated with broadband light. Even at one incident wavelength, light can be coupled to any non-resonant modes in a multimode waveguide through scattering, decreasing the light available for resonant reflection. Controlling scattering losses, so that the resonance effect will be most efficient, is possibly the greatest hurdle. We expect the SiO_2 deposited and etched grating to be the most significant contributor to scattered light, due to bulk scattering and scattering at the etched grating walls. Because of this, the RSG design utilizes a two-layer configuration and confines most of the resonant field in the waveguide layer, with only a small tail extending into the grating region.

2. Theoretical Predictions

This section contains most of the theoretical treatment of the RSGs. The first subsection uses rigorous coupled wave analysis (RCWA)[8] to predict the response of an RSG with infinite lateral extent when a plane wave is incident. This behavior is the limiting response of the component. Subsection 2.2 describes theoretical results when the incident beam has a finite width, such as a Gaussian beam or an apertured plane wave. This treatment again utilizes RCWA since the RSG is still infinitely large and the incident beam may be modeled as an

angular spectrum of plane waves. Subsection 2.3 contains predictions for a comparable configuration using the Helmholtz Equation code. Finally, subsection 2.4 quantifies the effects of limiting the grating width while keeping the waveguide infinite, and continuing to use a relatively large incident beam.

2.1 Infinite Extent RSG with Incident Plane Wave

If the RSG is assumed to have an infinite lateral extent and the incident beam is a plane wave, then the device may be modeled using rigorous coupled wave analysis (RCWA). Under these assumptions and with normal incidence, the reflectivity of the device reaches 100% at the resonant wavelength of 849.05nm as shown in Figure 3. The FWHM of the peak is 1.66nm. Note that the off-resonance reflectivity is low, with the maximum reflectivity outside the central peak being 4.3% at 1.0μm.

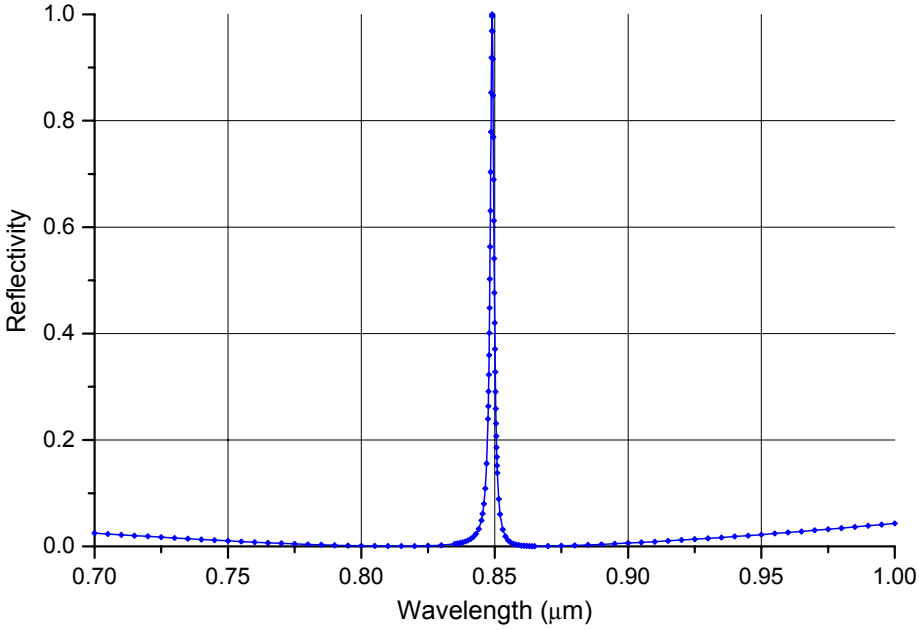

Figure 3 Reflectivity of an infinite RSG with normally-incident TE plane wave excitation, calculated using rigorous coupled wave analysis.

2.2 Finite Beam Using RCWA on Infinite RSG

Changing the angle of incidence from the normal to small off-axis angles has a profound effect on the spectral response of the RSG. Figure 4 shows the reflectivity as a function of angle of the incident plane wave from the normal for the case of an infinite-extent RSG, calculated using RCWA. Darker grays on the graph represent higher reflectivity. It is clear that at very small angles from the normal a second peak develops at a shorter wavelength, while the first peak shifts to a longer wavelength. As the angle is increased, these two peaks diverge in wavelength. Both peaks have a reflectivity at their respective maxima of 100%;

however, at small angles the shorter wavelength peak is considerably narrower in width than the longer wavelength peak (at 0.1º from the normal the FWHMs are 0.19nm and 1.46nm for the short and long wavelength peaks, respectively). At larger angles, the peaks become more comparable in width. For the design wavelength of 849.05nm, the reflectivity quickly falls off for even small angles.

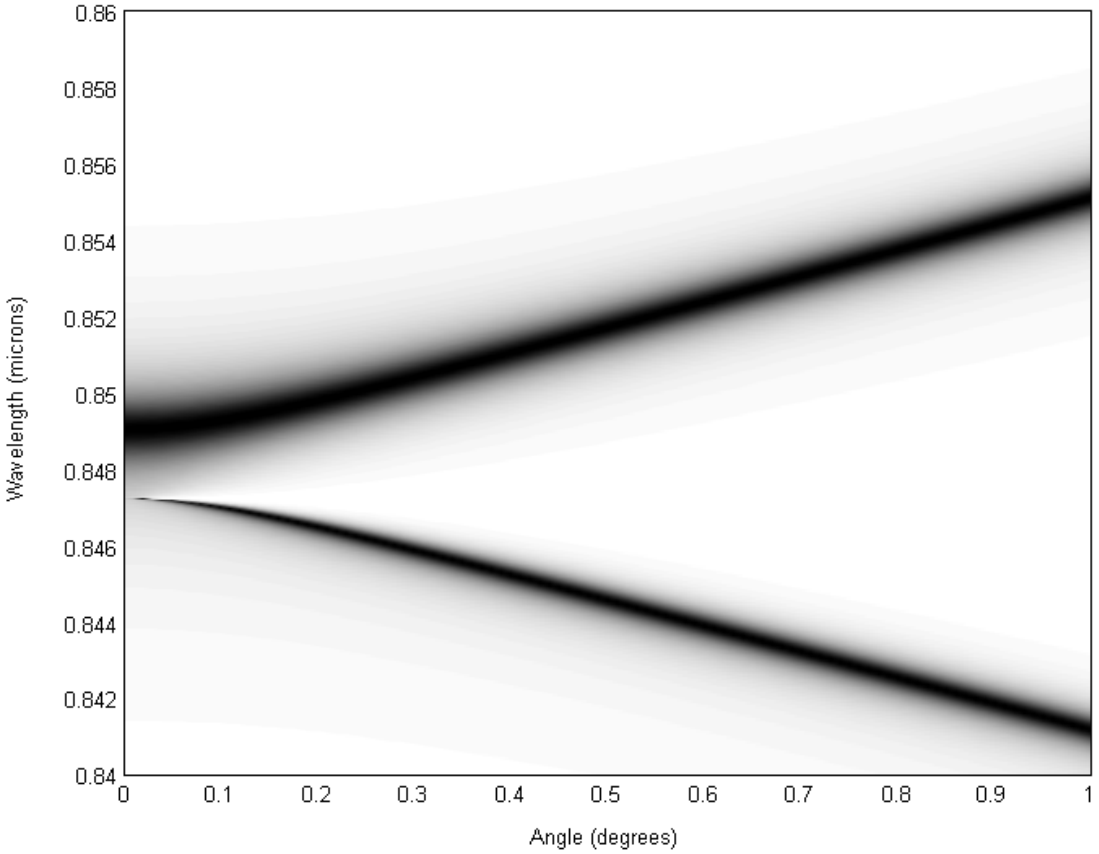

Figure 4 Reflectivity of a plane wave from an infinite-extent RSG as a function of incident angle from the normal: dark color indicates high reflectivity.

The RCWA angular data presented graphically in Figure 4 may be used to consider a normally-incident, finite-extent Gaussian beam on an infinite RSG. A normally incident finite Gaussian beam will contain angular components centered about, but not limited to, zero degrees. As the angle over which the RSG reflects a given wavelength is generally very narrow some of the energy in a finite beam will not be reflected, thus lowering the efficiency of the RSG. Decomposition of a Gaussian into its plane wave components in a manner such as that of Magnusson[9] allows RCWA to be used to analyze a Gaussian beam through its plane wave angular components. Consider a Gaussian beam of the form shown in Equation (1).

$$E(x) = Ae^{-\left(\frac{x}{a}\right)^2}, \tag{1}$$

where a is the half-width of the field, and A is a constant. Taking the Fourier transform of this equation to obtain the angular spectrum results in

$$F(\theta,\lambda) = A'\pi a e^{-\left(\frac{\pi a\theta}{\lambda}\right)^2}. \tag{2}$$

The Gaussian may now be approximated with plane waves over the range of angles in the angular spectrum of the Gaussian weighted according to Equation (2). The reflectivity, *R(θ)*,of the RSG as a function of angle is easily calculated for plane waves and infinite extent gratings using RCWA. For a given finite Gaussian, an approximation of the reflectivity is thus the product of the plane wave reflectivity and the angular spectrum of the Gaussian squared.

$$R = \int F^2(\theta,\lambda)R(\theta)\,d\theta \tag{3}$$

Results of the Gaussian beam decomposition method are shown for a range of beam input widths in Figure 5.

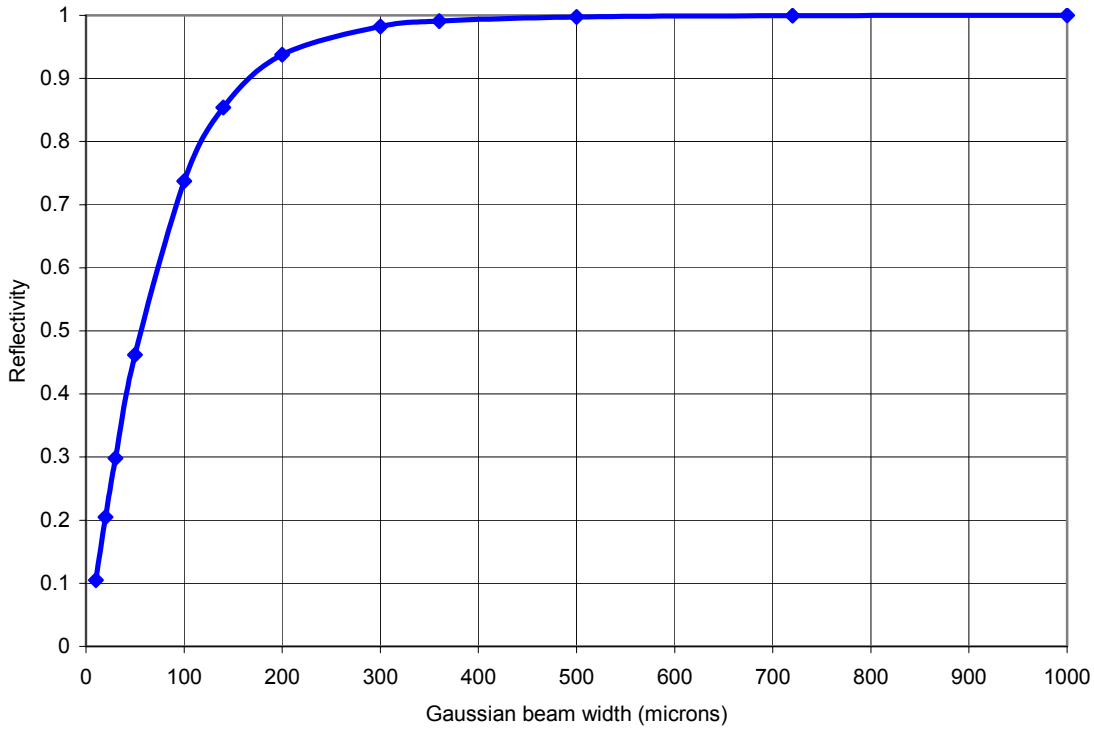

Figure 5 Reflectivity of an infinite RSG at 849.05nm as a function of Gaussian beam width (width measured between $1/e^2$ points of the beam intensity) determined with weighted-RCWA technique.

2.3 Finite Beam on Large RSG Using Helmholtz Equation Code

It is expected that if the beam or the grating is of finite extent then the peak reflectivity decreases, coupled with an increase in the spectral FWHM and a shift of the resonant wavelength. To model the finite gratings we used a finite difference implementation of the two-dimensional semi-vectorial Helmholtz equation. The dimensions of these structures are particularly well suited to the direct-matrix inversion employed in the Helmholtz code. A grating structure may be over 1mm long, but only a few microns are required in the y dimension. The solution time and memory requirement scales linearly with the larger dimension, but super-linearly with the smaller dimension. Fortuitously, the long, but narrow, simulation region of the single-mode waveguide RSG exploits this efficiency. We will now consider the case of a finite beam size in the form of a Gaussian beam, while maintaining a waveguide of infinite length using a method to be described below.

Modeling of this configuration may be accomplished with two-dimensional finite difference Helmholtz code utilizing the configuration shown in Figure 6. A symmetry boundary condition in used on one side, allowing the doubling of the size of the RSGs modeled for given memory and processor time. Absorbing boundaries are used to absorb unwanted reflections back from the RSG and energy exiting the end of the waveguide. A radiation boundary comprises the final boundary for energy that passes through the RSG. As in the RCWA case, the simulation is two-dimensional, thus the grating ribs are assumed infinite in the z dimension.

To approximate the infinite RSG lateral extent modeled with RCWA in the previous section, the RSG is extended into the absorbing boundary. Thus, energy remaining in the waveguide at the termination of the grating is absorbed in the boundary and does not reflect or otherwise interact with RSG operation. The imaginary component of the refractive index in the absorbing regions is ramped parabolically along x to minimize the reflections into the waveguide. A Gaussian beam centered on the symmetry boundary forms the input. The beam sizes considered here are sufficiently smaller than the size of the RSG such that by the onset of the side absorbing region the field strength is orders of magnitude smaller than the peak field strength. Results of the Helmholtz code to the RCWA results should thus be comparable.

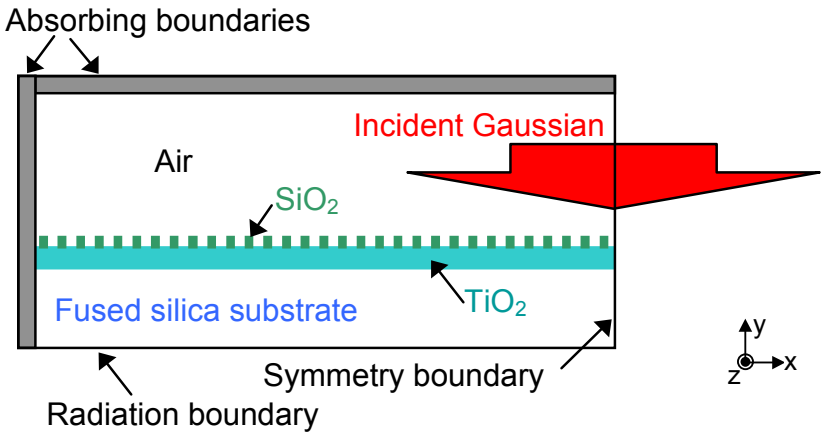

Figure 6 Configuration for finite difference method Helmholtz computations.

Results of the Helmholtz modeling of the RSG illustrated in Figure 7 are qualitatively similar to those obtained with RCWA, shown in Figure 4. In Figure 7, with decreasing beam width the primary resonant peak can be seen to shift to a longer wavelength. As it does so, the peak widens and the peak reflectivity drops. In addition, the appearance of a secondary peak occurs at shorter wavelengths, which shifts to increasingly shorter wavelengths with decreasing beam width. All of these features were also predicted by the RCWA calculations. A direct comparison is shown in Figure 8 for the case of a beam width of 200μm. While similar features appear on both curves, they appear at slightly different frequencies and amplitudes. This disparity may in part be due to the sensitive nature of modeling resonant devices, where discretization and boundary conditions can slightly shift resonant effects. In all of the cases we modeled, an approximate shift of 0.4nm to a longer wavelength was seen in the Helmholtz results compared to similar RCWA simulations.

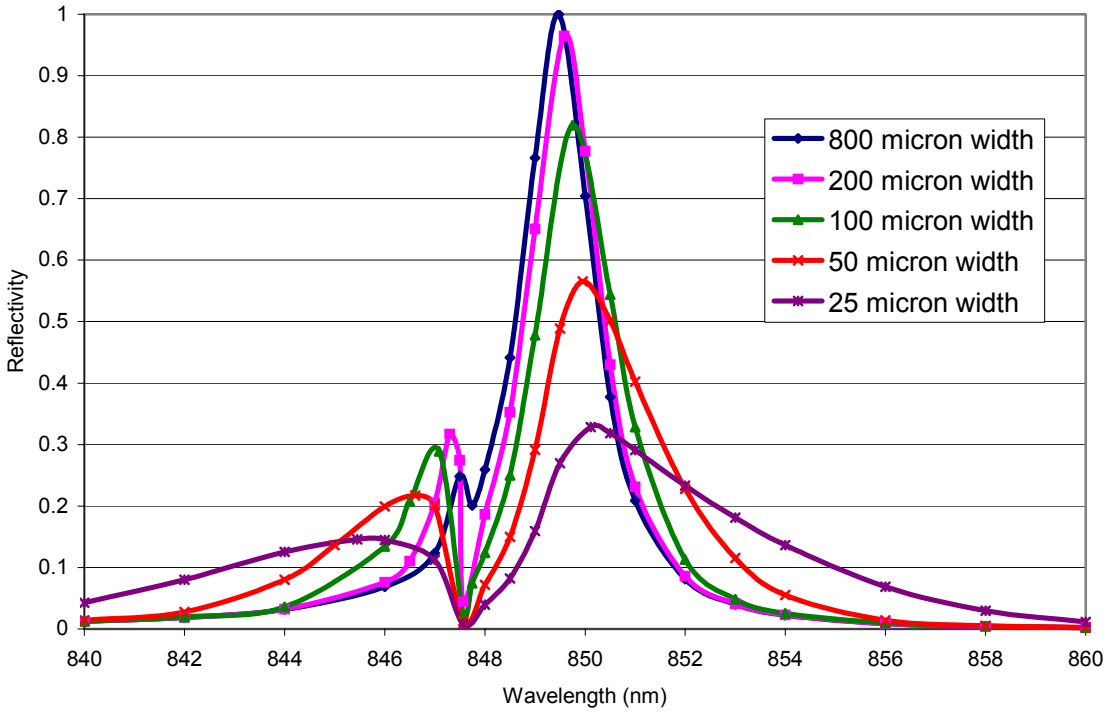

Figure 7 Spectral response of RSG as a function of limited-extent Gaussian beam width calculated with FDM Helmholtz equation.

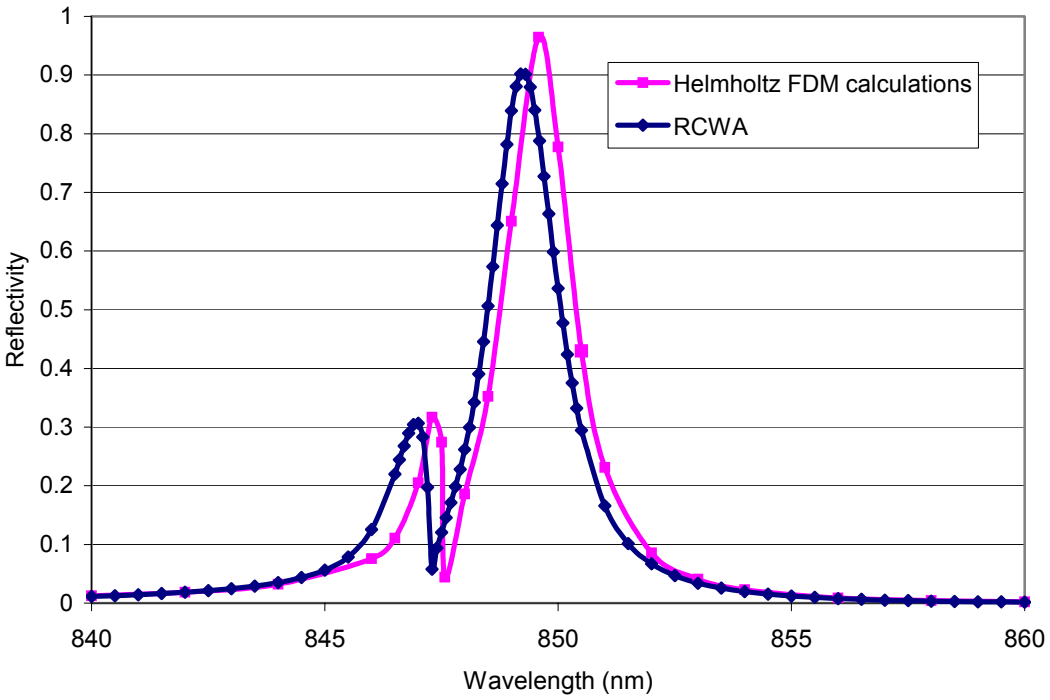

Figure 8 Spectral response of a 200µm width Gaussian beam using RCWA with plane wave decomposition and the FDM Helmholtz method on a 1.22mm-wide RSG.

2.4 Varying Grating Width with Infinite Waveguide and Large, Fixed Beam Size

We will now consider the case of a finite number of grating periods, while maintaining a waveguide of infinite length and a large, constant Gaussian beam width. We may thus consider the effect of a limited number of etched grating teeth on the reflectivity of the RSG. With the grating restricted in lateral extent, guided energy in the waveguide layer may continue to propagate past the grating termination. This energy is not recoupled by the grating to backward-radiated energy, and thus not reflected. This guided-mode energy is trapped in the waveguide and is energy lost from the system; the amount of this energy loss is dependent on the grating strength and lateral extent, as well as the size of the incoming beam.

Modeling this configuration may be accomplished with the two-dimensional finite difference Helmholtz code utilizing the configuration shown in Figure 9. All boundary conditions and materials are the same as in Figure 6, the difference being the form of the grating layer. Here the etched grating has a finite width, however the waveguide is allowed to extend to the absorbing boundary. For these calculations a 1.22mm wide simulation region was used. Guided-mode energy propagating in the waveguide will be dissipated in the absorber, mimicking the energy lost in the infinite waveguide. The grating is centered in the RSG, with the size varying. Outside the grating width, the SiO_2 layer is left unetched.

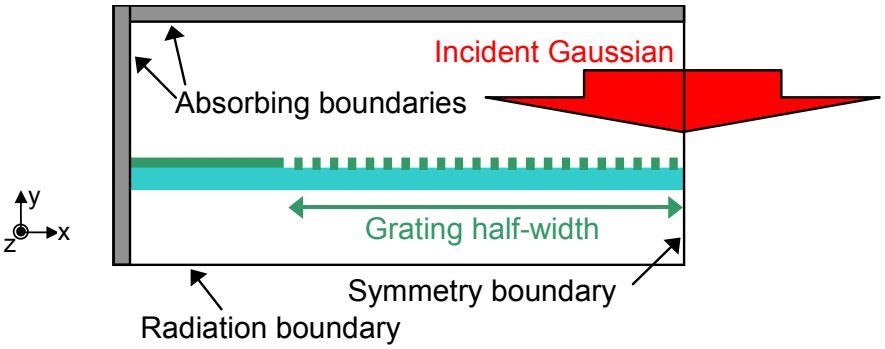

Figure 9 Simulation format used to determine reflectivity of finite grating RSG.

The beam is a normally-incident Gaussian with a width between e^{-2} power points of 800µm. The use of a wide beam minimizes the effect of non-zero angular components, with the power in the angular spectrum falling to half by 0.4mrad. This allows the investigation of the finite grating effect independent of finite beam effects. However, the beam is narrow enough to avoid interference with the side absorbing boundary conditions.

For the finite grating, the peak reflectivity drops below 100%, which was the case for the infinite-extent grating. However, for the 1mm wide grating a curve very close to the RCWA infinite grating/plane wave input case is obtained, as seen in Figure 10. Wavelength regions outside the central 20nm region plotted in Figure 10 show minimal variation from the RCWA results in Figure 3. At the opposite extreme, the case of no grating results in the expected reflectivity of a thin film stack. Note that the off-resonance reflectivity from the larger gratings result in lower reflectivities than the thin film case as the thickness of the SiO_2 layer was chosen to minimize reflectivities in this range with a grating present[7]. As the grating width shrinks the peak continues to drop from unity.

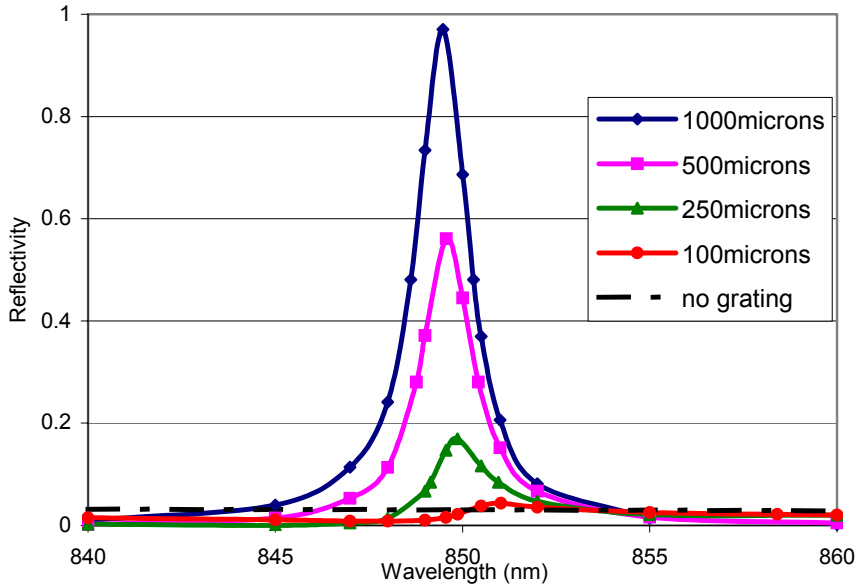

Figure 10 Reflectivity from several finite grating widths in a fixed simulation region of 1.22mm and using a large, fixed incident 800µm width Gaussian beam.

A key difference between the effect of a finite beam and the effect of a finite grating can be seen in comparing the results of Figure 10 to those of Figure 7. In the finite beam case the lowering of the peak reflectivity and broadening of the resonant peak is coupled with the appearance of a secondary peak at shorter wavelengths, the result of non-zero angular components present in the finite beam. In the case of the finite grating, where a wide, constant Gaussian beam is used as excitation, we see a similar decrease in peak reflectivity and increase in peak width. However, we do not see the secondary peak appear. This is the result of the input beam remaining constant, with no change in the angular components of the beam.

In addition to the decrease in peak reflectivity, a shift to longer wavelengths in the peak reflectivity is also apparent. With decreasing grating width, the peak reflectivity monotonically decreases as shown in Figure 11. As the grating width approaches zero, the reflectivity approaches the reflectivity expected from the unetched SiO_2 and TiO_2 films on fused silica of 3%. Concurrently, the FWHM increases with decreased grating width as shown in Figure 12; the curve shown is an exponential fit.

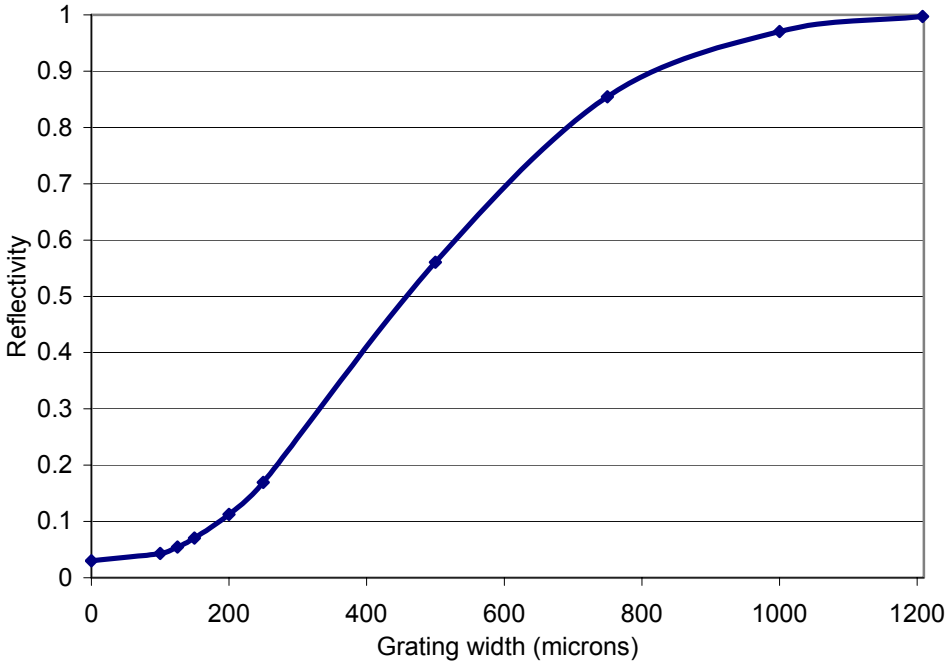

Figure 11 Spectral peak reflectivity as a function of grating width for case of a large, fixed Gaussian beam and fixed simulation region.

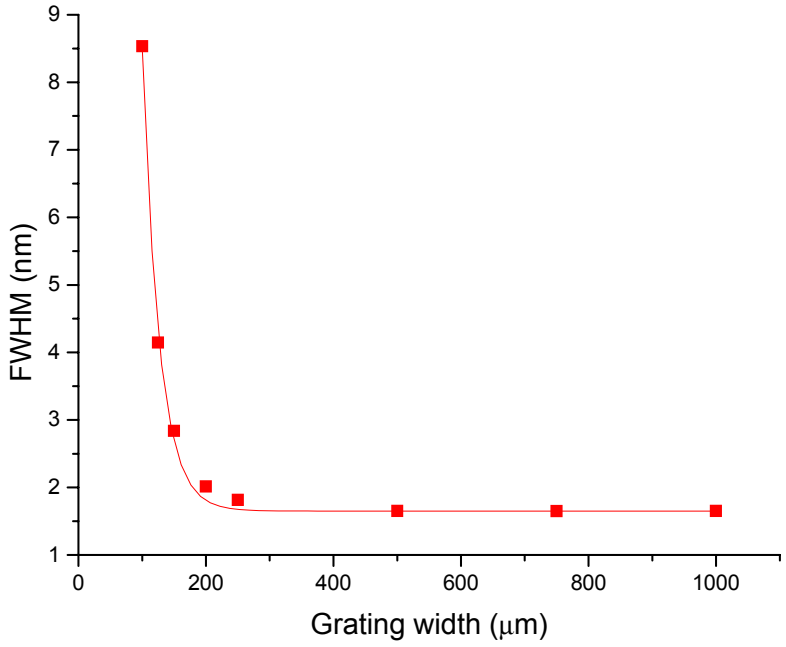

Figure 12 Spectral full width at half maximum of reflectivity response as a function of grating width for case of large, fixed beam size and fixed simulation region (Note: Fitted curve is an exponential with $\alpha = 0.039\mu m^{-1}$).

3. Measured RSG Spectra

This section contains the measured results from the previously designed and fabricated RSGs. The first subsection shows spectra with remarkably high reflectivity obtained from a large area RSG. Subsection 3.2 demonstrates the effect of limiting the RSG aperture on reflectivity and spectral full width at half max. Finally, subsection 3.3 contains RSG spectra for non-zero angles of incidence. These are measured on a large area RSG as well as a limited extent RSG.

3.1 Large Area RSG with Normally Incident Light Measurements

Figure 13 shows our exciting experimental results where the peak reflectance reaches 100.2% normalized to bulk, deposited gold. Predicted gold reflectivity reaches 99.4% at these wavelengths so we may conclude that this device demonstrates comparable or better reflectivity than the published record of 98%[10]. The spectral FWHM is a narrow 4.14nm and perhaps more importantly, the sidebands across the wide spectral range remain low and flat (≤5%); close to our theoretical target of 4.3%.

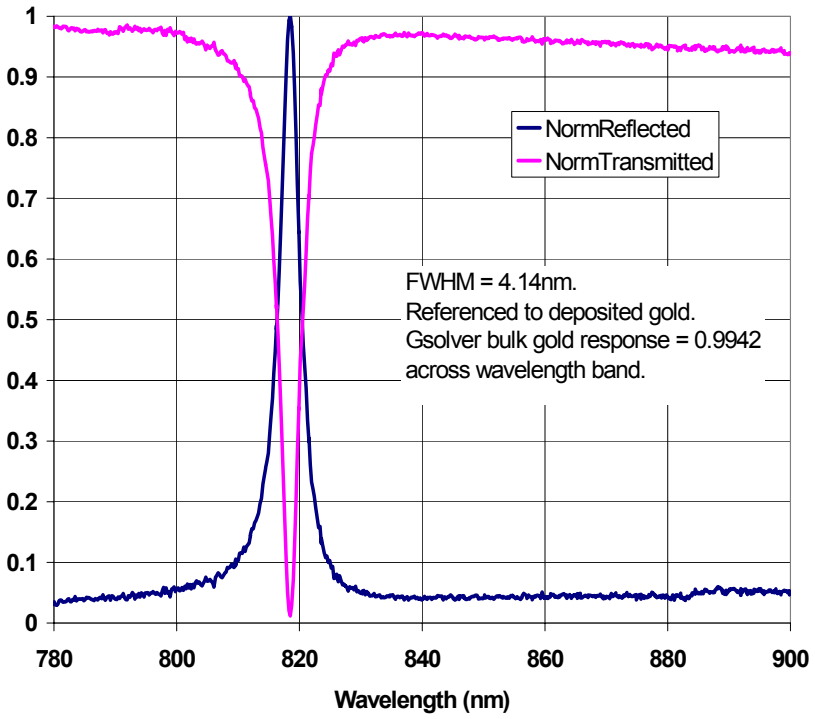

Figure 13 Measured reflected and transmitted RSG spectra with normally incident light. Reflectivity measures 100.2% relative to bulk gold.

These large area RSG measured results were obtained with (an apertured, 1mm diameter) plane wave input on a 2X2mm RSG in an effort to confirm predictions for a component with infinite lateral extent. However, in an integrated RSG array configuration, each pixel in the array must be small enough so that the entire array extent is compact. Pixel dimensions of 100-300μm are within the targeted range. This design consideration presents a considerable challenge. Peak reflectance is expected to decrease with an accompanying increase in spectral FWHM as the pixel lateral extent decreases[11-16]. On the other hand, smaller, arrayed RSG configurations are more easily integrated with existing sensing and detecting arrays. Here, applications include narrow band filter arrays for fluorescence detection or single-chip integrated spectrometer detection arrays. The trade-off between configuration utility and device performance is quantified in this project.

3.2 Finite Aperture RSG with Normally Incident Light Measurements

Figure 14 shows the expected decrease in measured peak reflectance as a function of RSG lateral extent for a normally incident plane wave. Again the light is a normally incident plane wave that is stopped down to a 1mm diameter at the RSG. Each RSG pixel has a continuous substrate and waveguide lateral extent, but the grating extent in the direction perpendicular to the grating grooves is limited. The grating dimensions are: 2.00mmX2.00mm, 0.96mmX2.00mm, 0.48mmX2.00mm, 0.24mmX2.00mm, 0.16mmX2.00mm, and 0.08mmX2.00mm for devices 1-6, respectively. The incident spot overlap is essentially 1mm in diameter for the largest two devices, but significantly overfills the width of the other four

smaller devices. Thus some incident light on devices 3-6 falls upon the TiO2/fused silica substrate and that portion of the incident light does not contribute to resonant reflection. The subsequent reflectivity values are still normalized to the 1.00mm incident spot irradiance, resulting in efficiency measurements that are underestimated when compared to efficiency measurements with matching incident and diffracted areas. The experimental spectra shown in Figure 14 are directly comparable to the predicted spectra in Figure 10.

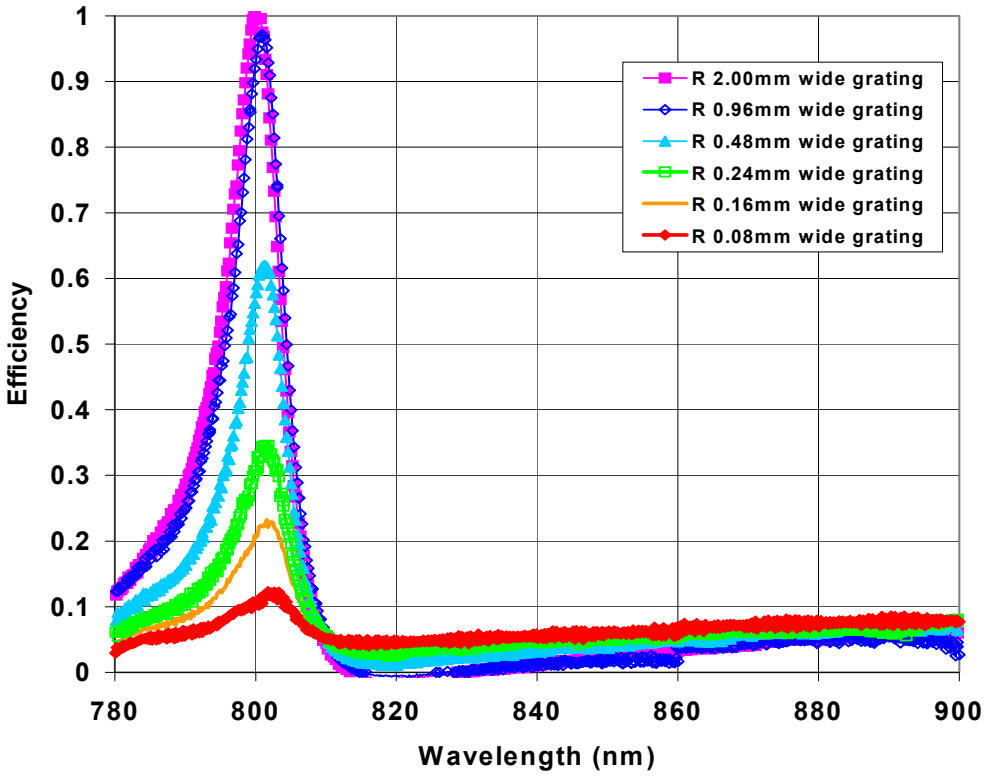

Figure 14 Measured reflectance spectra for a fixed-width normally incident beam on RSG pixels with decreasing grating width.

Figure 15 contains the measured peak reflectivities from the above data and compares these to values modeled with a finite difference implementation of the two-dimensional semi-vectorial Helmholtz code[17] from Figure 11. The modeled points are for a 1.0mm wide Gaussian beam and the measured data are for a 1.0mm wide apertured plane wave.

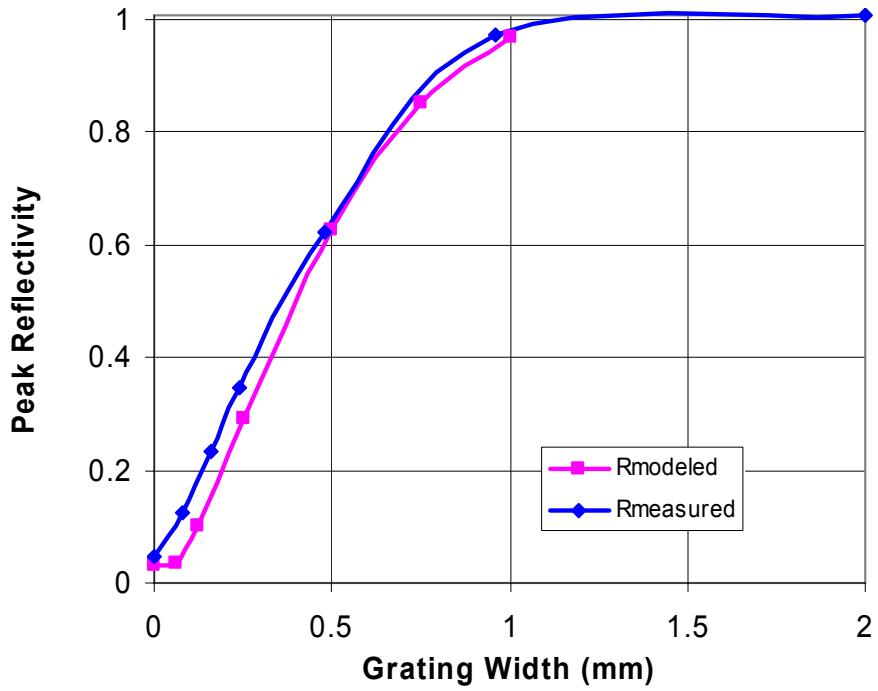

Figure 15 Experimental and measured peak reflectivities as a function of grating width for a large, fixed-width, normally incident beam.

3.3 Nonzero Angles of Incidence on RSGs

All of the previous measurements are in symmetrical experimental configurations; the beam is normally incident and the grating profile is rectangular. Thus there is no reason to expect but a single peak in the spectra. However, changing the plane wave angle of incidence breaks the symmetry by launching two different mode angles from the grating into the waveguide. At the appropriate wavelengths, a mode will resonate and the resulting spectra will contain two peaks. This is evident in Figure 16 where the highest reflectivity is displayed as black and lowest reflectivity is white.

This simulation, as a function of angle of incidence and the resulting wavelength, is for RSGs of infinite lateral extent and is centered about a slightly different wavelength than our measurements because the modeled grating pitch is larger. Still, the behavior will be comparable to measurement; on axis there is only one peak that splits into two as the beam is moved off axis.

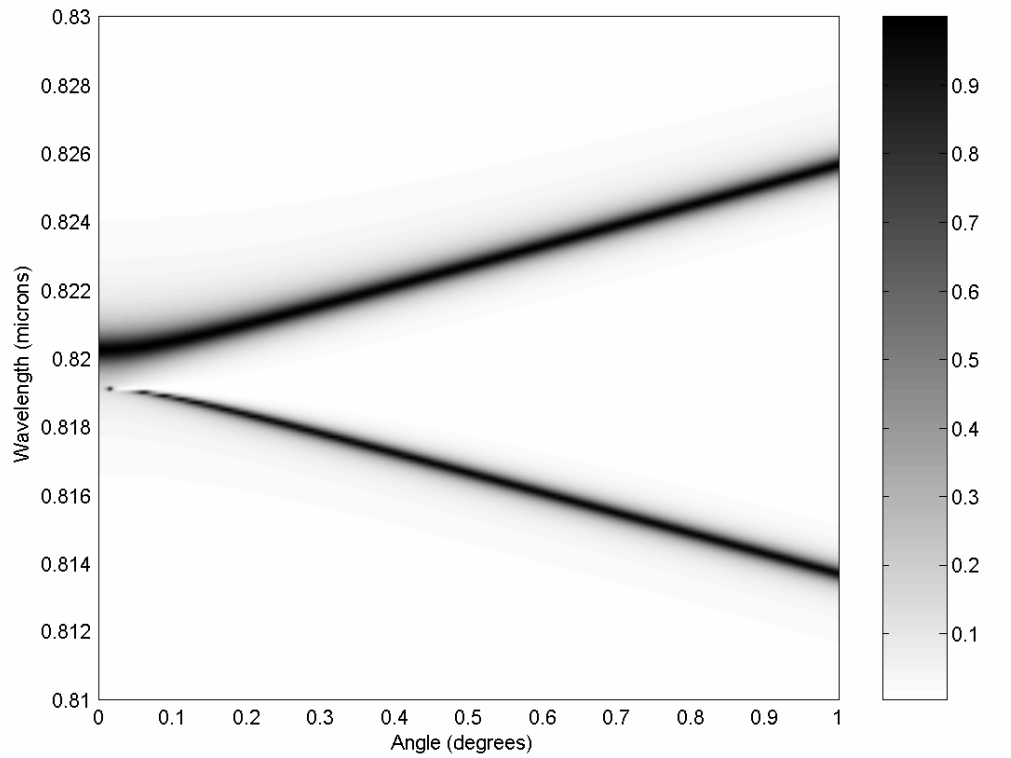

Figure 16 Reflectivity spectra for a plane wave at various angles of incidence. High reflectivity is mapped to dark grays.

These simulation results are confirmed in the measured spectra in Figures 17(a) and 17(b) for incident angles ranging from zero to two degrees. The results for negative angles were identical within experimental error. The measured spectra are for the 1mm diameter apertured plane wave incident upon the largest, 2.00mm X 2.00mm, RSG pixel. As the beam moves from normal to a positive angle a second, smaller peak emerges at the lower wavelengths. Even a variation from normal as small as 0.1 degrees causes a second peak to just appear.

The same spectra were measured on device 4, a smaller 0.24mm X 2.00mm RSG pixel, to quantify any changes due to the limited RSG extent and are shown in Figures 18(a) and 18(b). The double peaked spectra for this finite aperture RSG appear to be just a lower efficiency version of the larger aperture results in Figure 17.

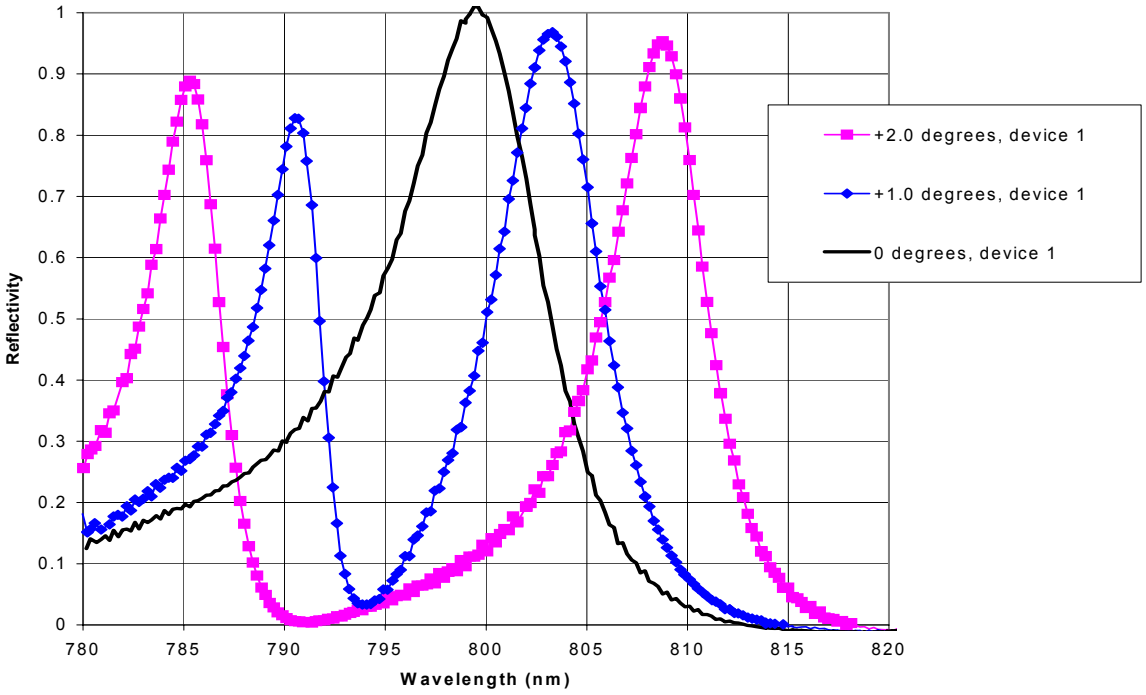

(a)

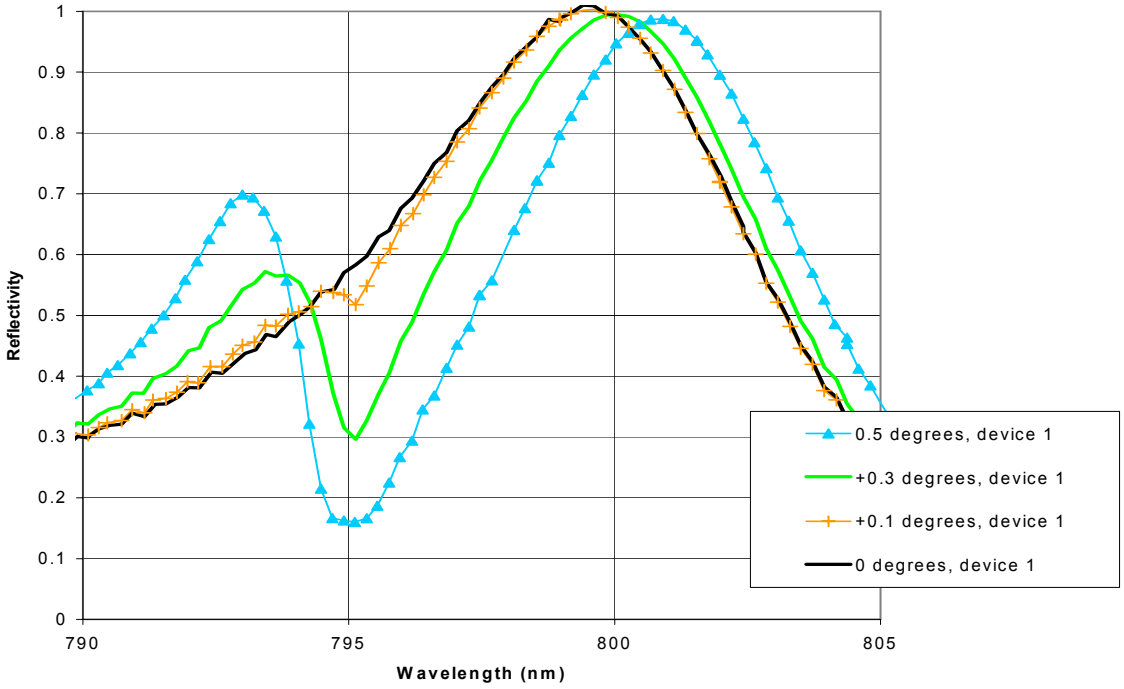

(b)

Figure 17 Measured RSG spectra for plane waves at various angles of incidence on the largest (2.00mm X 2.00mm) RSG device 1 for (a) larger incident angles, and for (b) incident angles close to zero.

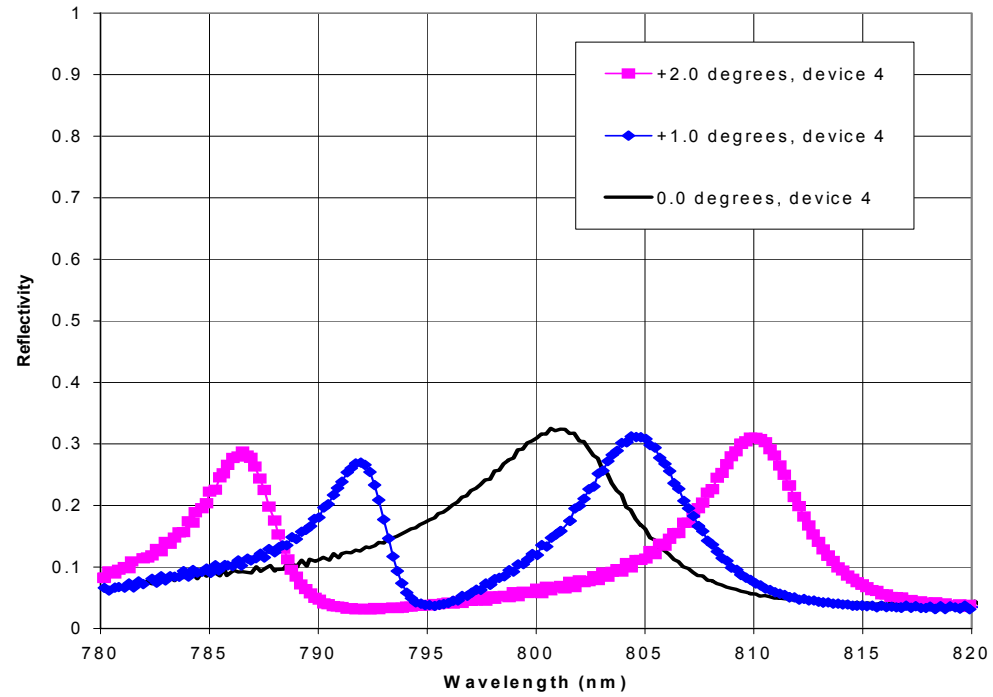

(a)

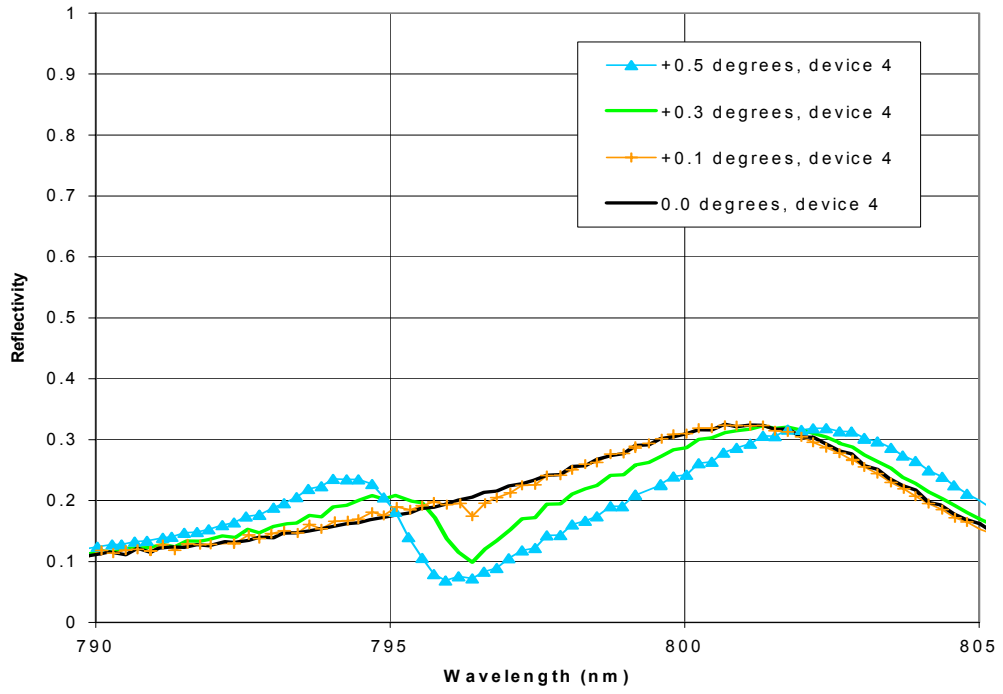

(b)

Figure 18 Measured RSG spectra for plane waves at various angles of incidence on the smaller (0.24mm X 2.00mm) RSG device 4 for (a) larger incident angles, and for (b) incident angles close to zero.

This apparent similarity in spectra is confirmed in Figure 19 where the wavelength difference between the two reflectance peaks is plotted as a function of incident angle for the larger RSG (2.00mm X 2.00mm) as well as the limited extent (0.24mm X 2.00mm) RSG. The linear relationship is the same, regardless of aperture dimension.

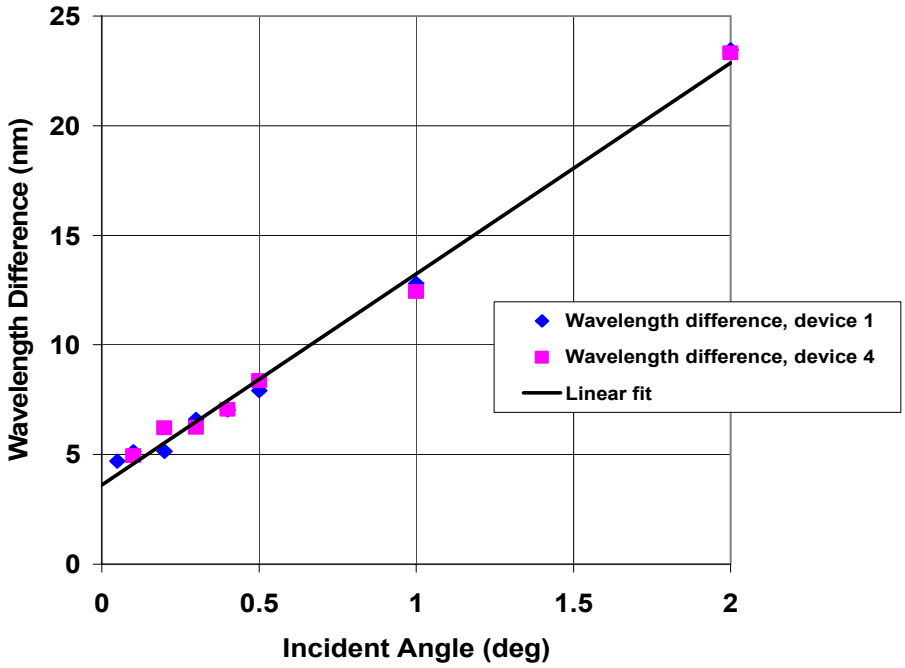

Figure 19 Wavelength difference between double reflectivity spectral peaks as a function of plane wave incident angle for a large and finite aperture RSG.

4. Theoretical Predictions of Feedback Effects in a Finite Grating and Finite Waveguide

In a finite-sized device, the waveguide layer must be terminated at a point at, or at some distance after, the end of the grating as illustrated in Figure 20. The form of this termination may greatly affect the overall efficiency of the grating. This distance has a large effect on the reflectivity of the device as the reflection of the guided mode from the end facet of the waveguide either may constructively or destructively interfere. This effect is most pronounced when the incident beam is approximately the width of the grating. In this case, the field strength is still significant at the edge of the device.

For an RSG in an array, the incident energy will be a truncated plane wave. To simulate this effect, a rectangular beam with a width equal to the width of the grating is used as the input beam.

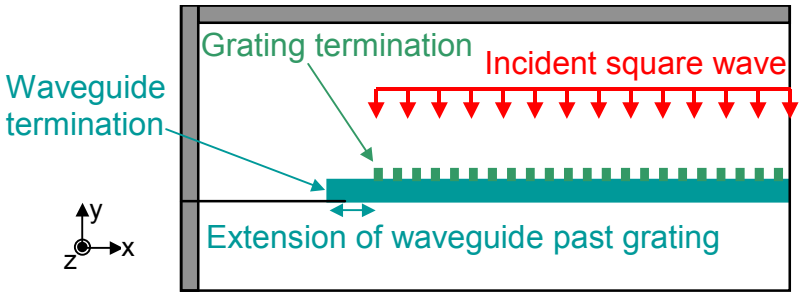

Figure 20 Finite grating and finite waveguide layer (boundary conditions identical to Figure 6).

The reflectivity was determined for a set of RSGs that are identical except for overall length of the guiding layer. We calculate the reflectivity with the guiding layer termination in line with the final grating ridge, then extend the guiding layer past the termination of the grating. In Figure 21 the reflectivities of the RSGs are plotted as functions of grating width and the extension of the waveguide past the grating. The oscillatory nature of the reflectivity is clear, with the maximum occurring when the waveguide and grating layers are terminated at the same point. The amplitude of this variation peaks with gratings whose width lead to reflectivities around 0.5. For gratings in this regime, a difference in reflectivity of 30% occurs with a submicron change in the length of the waveguide with respect to the grating.

In Figure 22, we compare the case of the infinite waveguide to the case of the waveguide and grating layers terminated at the same distance. In general, the reflectivity from a finite-extent waveguide RSG may be higher or lower than the infinite-waveguide RSG. However, for the case of termination of the waveguide in line with the grating, the reflectivity in the finite case is maximized and is always greater than the infinite-waveguide RSG. This feedback effect is more pronounced in waveguides with higher indices of refraction and greater Fresnel reflections from the end facets.

The feedback also acts to reduce the full width at half maximum of the spectral response as seen in Figure 23, particularly for shorter grating widths. While the FWHM decreases, the change from an infinite to finite guiding layer does not significantly affect the resonant wavelength. This beneficial result allows the use of feedback to increase the reflectivity and decrease the width of the response while not shifting the resonant frequency.

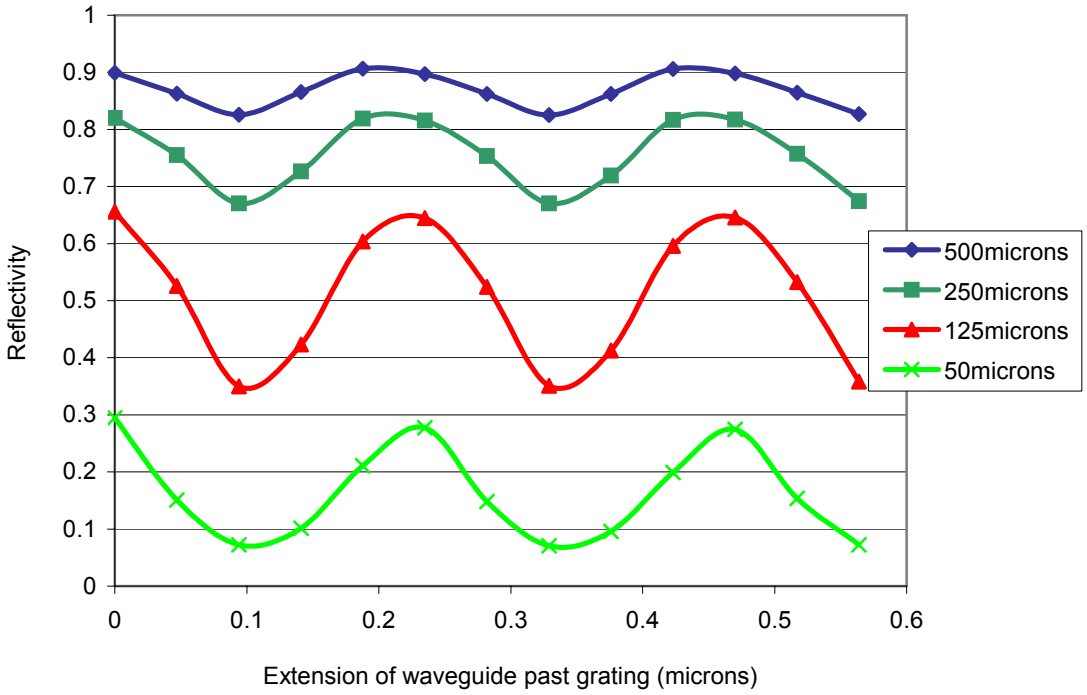

Figure 21 Peak reflectivity as a function of the extension of the finite waveguide past the termination of the finite grating for five grating and square incident wave widths.

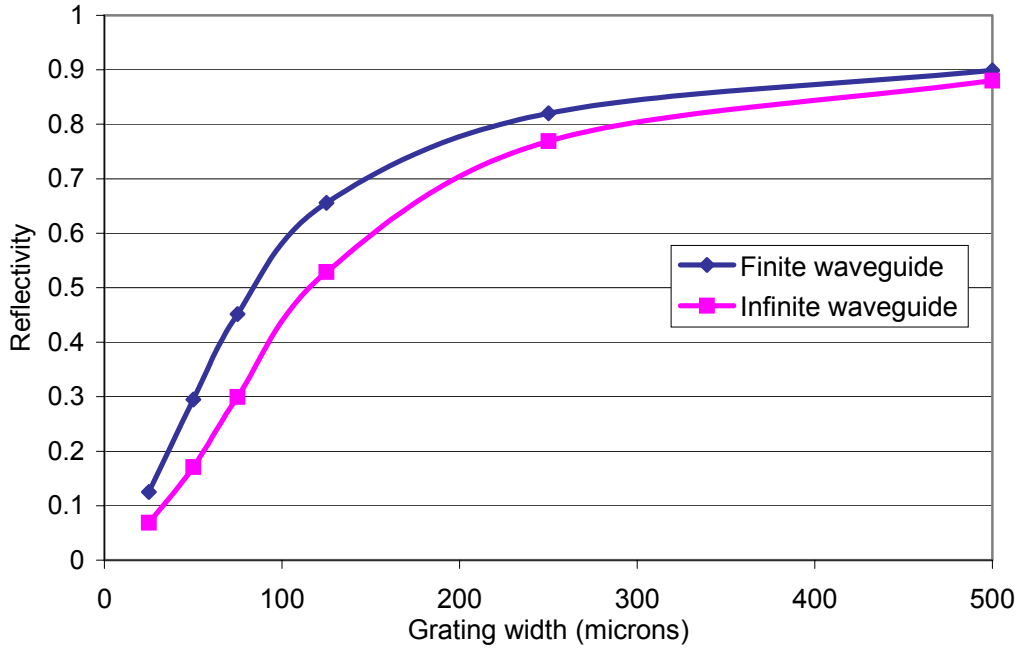

Figure 22 Reflectivity from an RSG with the waveguide terminated at the end of the grating compared to the reflectivity from the same RSG with the waveguide extended to infinity.

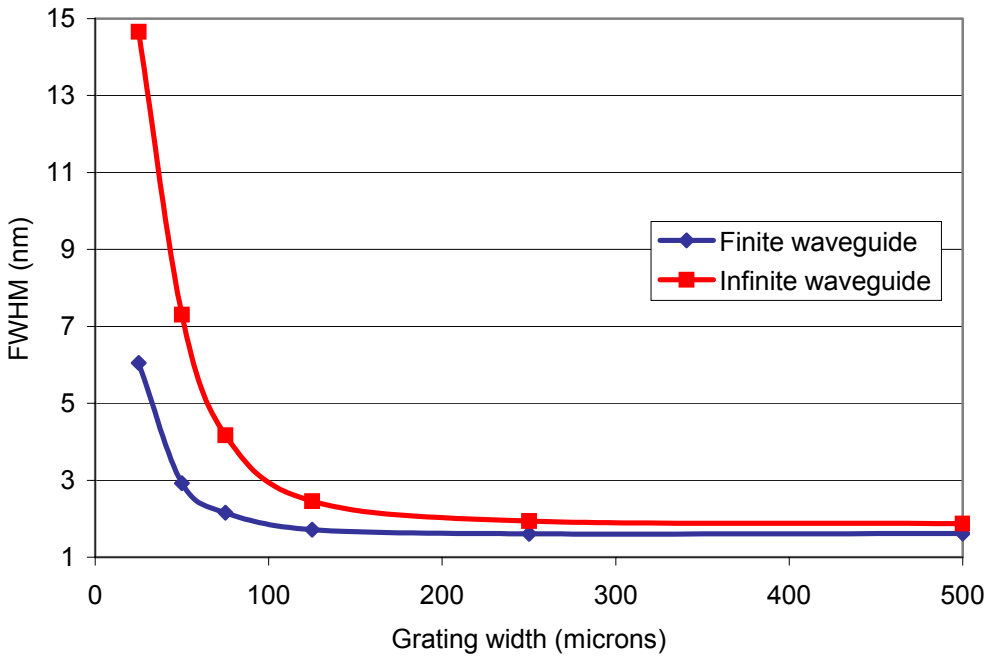

Figure 23 Full width at half maximum as function of the grating width for a finite grating on an infinite waveguide and a finite grating on a waveguide terminated at last grating ridge.

5. Conclusions

The arrayed resonant subwavelength grating (RSG) utilizes a remarkable individual component with predicted efficiency of 100%. Incorporating this component into a limited extent format will result in expected reduced peak efficiency. We have theoretically and experimentally characterized these issues for an RSG in the near-IR wavelength regime.

We used FDM Helmholtz equation simulations to model finite size resonant subwavelength gratings. These rigorous numerical calculations are compared to simulations of their infinite-extent counterparts. The spectral response for the case of a finite beam width and for a finite grating width show similar traits in that with decreasing size of the beam or grating the peak reflectivity shifts to a longer wavelength and decreases in magnitude. Likewise, the peak broadens as the size in either case is decreased. However, the appearance of a secondary peak is limited to the case of the finite beam and may be explained by the inclusion of non-zero angular components in any finite beam.

Aperturing an input plane results in an exponential shift in the resonant wavelength as the aperture width decreases. Peak reflectivity suffers a similar exponential decrease as aperture width narrows. Arrays of such devices, where apertured input is mandatory, will therefore be difficult at small sizes except for the strongest of coupling gratings.

We fabricated and characterized several large area (>1.00mm diameter) RSGs with reflectivities as much as 100.2% relative to deposited, bulk gold. Moreover, the sidebands

were flat and <5% across the 300nm wavelength band. The spectral FWHM was as low as 4nm, but was double that for the wafers with varying aperture widths. Decreasing the RSG aperture width while keeping the incident beam diameter large (1.00mm) reduced the peak reflectance from 100.2% to 63% to 34% to 12% for aperture widths of 2.00mm, 0.48mm, 0.24mm, and 0.08mm, respectively.

Measured spectra for non-zero plane wave incidence angles confirmed theoretical predictions that a system asymmetry introduced a second peak in the reflectance spectrum. This is predicted in infinite extent RSGs and remains the case when the RSG aperture is of finite extent. The measured wavelength separation between the two peaks is a linear function of incidence angle for the angles between +/-2.0 degrees. The second peak emerges at an off-normal incidence angle as low as 0.1 degrees. These results for non-zero incidence angles are independent of aperture size, and would also be evident in a multiple k-vector converging or diverging incident beam configuration.

Helmholtz simulations predict finite gratings have a reduced reflectivity, and that this reflectivity is highly dependent on the method with which the grating and/or waveguide is terminated. Reflection from the end facet of a waveguide termination may either enhance or degrade the reflectivity compared to the reflectivity of a structure with a similar finite grating, but with infinite waveguide. Enhancement or degradation is determined by whether the reflection from the end facet is in-phase or out-of-phase with the reflections from the grating feedback. Dependence of the reflectivity is near sinusoidal with the length of the grating. Maximum effect of the end-facet termination is seen in finite-extent devices with reflectivities near 50%, where a 30% variation in reflectivity is evident with small changes in the end facet dimensions.

Reflectivity from an end facet on the waveguide can also act to reduce the spectral width of the reflectivity. We have thus shown that end facet construction has a large effect on multiple figures of merit of the RSG element. This significant result illustrates the care that must be used in the design of finite RSGs as the result of an ill-designed edge termination can deleteriously affect RSG performance.

RSG simulations and measurements indicate that a large, resonant visible-to-NIR wavelength range (0.7 to 1.0 μm) is accessible, given material and fabrication restraints. The available materials in this wavelength regime are low refractive index contrast materials, causing the RSG characteristics such as peak wavelength and spectral response shape to be extremely sensitive to imprecision in fabrication and testing. Small changes in deposition thicknesses, refractive indices, grating period, and incident beam angles shift or reduce the resonance peak dramatically. While this makes fabrication and testing difficult, it speaks to the RSG's utility as a sensing component.

References

1. S.A. Kemme, M.E. Warren, W.C. Sweatt, J.R. Wendt, D.W. Peters, G.R. Hadley, T.R. Carter, S. Samora, D.W. Peterson, K.M. Geib, "Moving diffractive optical elements from stand-alone components into micro-optical systems," OSA Trends in Optics and Photonics, vol. 75, Diffractive Optics & Micro-Optics, Robert Magnusson, ed., Optical Society of America, Washington, DC, pp. 109-114 (2002).
2. S.A. Kemme, D.W. Peters, J.R. Wendt, T.R. Carter, S. Samora, G.R. Hadley, "Integration and tolerance issues for resonant subwavelength gratings," Proceedings of the SPIE Annual Meeting, San Diego, CA (August 2003).
3. D.W. Peters, S.A. Kemme, G.R. Hadley, "FDM Helmholtz modeling of finite grating and waveguide width effects on resonant subwavelength grating reflectivity," Proceedings of the SPIE Annual Meeting, San Diego, CA (August 2003).
4. S.S. Wang, R. Magnusson, J.S. Bagby, and M.G. Moharam, "Guided-mode resonances in planar dielectric-layer diffraction gratings," J. Opt. Soc. Am. A, vol. 7, pp. 1470-1474 (1990).
5. P. Vincent and M. Neviere, "Corrugated dielectric waveguides: a numerical study of the second-order stop bands," Appl. Phys., vol. 20, pp. 345-351 (1979).
6. I.A. Avrutskii and V.A. Sychugov, "Reflection of a Gaussian light beam from the surface of a corrugated waveguide," Sov. J. Quantum Electron., vol. 16, pp. 1558-1559 (1986).
7. D.W. Peters, S.A. Kemme, G.R. Hadley, "Low-sideband resonant subwavelength grating array design," OSA Trends in Optics and Photonics, vol. 75, Diffractive Optics & Micro-Optics, Robert Magnusson, ed., Optical Society of America, Washington, DC pp. 290-295 (2002).
8. M. G. Moharam and T. K. Gaylord, "Rigorous coupled-wave analysis of planar-grating diffraction," J. of Opt. Soc. Amer., vol. 71, pp. 811-818, (1981).
9. R. Magnusson and S. S. Wang, "Optical waveguide-grating filters" International Conference on Holography, Correlation Optics, and Recording Materials, O. V. Angelsky, ed., Proc. SPIE 2108, pp. 380-391, (1993).
10. Z.S. Liu, S. Tibuleac, D. Shin, P.P. Young, R. Magnusson, "High-efficiency guided-mode resonance filter," Opt. Lett, vol. 23, pp. 1556-1558 (1998).
11. D. K. Jacob, S. C. Dunn, and M. G. Moharam, "Normally incident resonant grating reflection filters for efficient narrow-band spectral filtering of finite beams," J. Opt. Soc. Am. A, vol. 17, pp. 1241-1249, (2000).
12. D. K. Jacob, S. C. Dunn, and M. G. Moharam, "Design considerations for narrow-band dielectric resonant grating reflection filters of finite length," J. Opt. Soc. Am. A, vol. 18, pp. 2109-2120, (2001).
13. R.R. Boye and R.K. Kostuk, "Investigation of the effect of finite grating size on the performance of guided-mode resonance filters," Appl. Opt., vol. 39, pp. 3549-3553 (2000).
14. J.M. Bendickson, E.N. Glytsis, T.K. Gaylord, D.L. Brundrett, "Guided-mode resonant subwavelength gratings: effects of finite beams and finite gratings," J. Opt. Soc. Am A, vol. 18, pp. 1912-1928 (2001).
15. J. Saarinen, E. Noponen, J. Turunen, "Guided-mode resonance filters of finite aperture," Opt. Engineer., vol. 34, pp. 2560-2566 (1995).

16. I.A. Avrutskii and V.A. Sychugov, “Reflection of a beam of finite size from a corrugated waveguide,” J. Modern Opt., vol. 36, pp. 1527-1539 (1989).
17. G. R. Hadley, "Low-truncation-error finite difference representations of the 2-D Helmholtz equation," Int. J. Electron. Commun. (AEU), vol. 52, pp. 310-316 (1998).

Distribution:

1	MS 9018	Central Technical Files, 8945-1
2	MS 0899	Technical Library, 9616
1	MS 0612	Review & Approval Desk, 9612 For DOE/OSTI
1	MS 0323	D. Chavez, LDRD Office, 1011
1	MS 0603	S. A. Kemme, 1743
1	MS 0603	D. W. Peters, 1743
1	MS 0603	J. R. Wendt, 1743
1	MS 0603	T. R. Carter, 1743
1	MS 0603	S. Samora, 1743
1	MS 0603	G. R. Hadley. 1742
1	MS 1202	M. E. Warren, 5911
1	MS 0972	C. L. Grotbeck, 5712
1	MS 0972	Andy Boye, 5710
1	MS 0603	Jim Hudgens, 1743